ELSEVIER

"The Microball"

Design, instrumentation and response characteristics of a 4π-multidetector exit channel-selection device for spectroscopic and reaction mechanism studies with Gammasphere

D.G. Sarantites [a,*], P.-F. Hua [a], M. Devlin [a], L.G. Sobotka [a], J. Elson [a], J.T. Hood [a],
D.R. LaFosse [a], J.E. Sarantites [a] M.R. Maier [b]

[a] Department of Chemistry, Washington University, St. Louis, MO 63130, USA
[b] Engineering Division Lawrence Berkeley National Laboratory, University of California, Berkeley, CA 94720, USA

Abstract

A 4π multidetector light-charged particle and light fragment detection spectrometer is described. It consists of 95 CsI(Tl) scintillators closely packed to cover the angular range 4.0°–172°, arranged in 9 rings with increasing forward segmentation. The device is optimally designed to be used in conjunction with Gammasphere. The scintillator light is collected by silicon photodiodes that provide high quantum efficiency and minimal mass. The signals are processed through a charge sensitive preamplifier followed by a slow shaper. Particle identification for ^{1,2,3}H, ^{3,4}He ions and Li, Be and B ions is accomplished by pulse shape discrimination. The geometry, construction, energy calibration, gain stability, associated integrated electronics and the data acquisition system are discussed. The capabilities of this spectrometer as a channel selecting device in conjunction with Gammasphere are discussed. A second version of the device with thicker scintillators, that can stop more energetic charged particles and is useful for reaction mechanism studies, is also described.

1. Introduction

In recent years, heavy ion induced reactions have provided a wealth of information about nuclear behavior at high spins and excitations. Discrete γ-ray spectrometry has employed a variety of multi-detector arrays to study exotic nuclear behavior. The most striking results of such studies include the recent observation of many superdeformed band structures [1,2] in nuclei. Heavy ion-induced fusion reactions generally produce neutron deficient compound nuclei with substantial charged particle and fission decay widths. In such cases, a large number of exit channels are populated and this renders difficult the selection of a particular channel for study. Spectroscopic studies of rare earth nuclei often employ γ-ray multiplicity gating techniques to select a specific xn channel. For nuclei with medium or low A, large cross sections for charged particle emission lead to many channels with similar γ-ray multiplicities which cannot be separated by γ-ray multiplicity gating. In such cases charged particle identification in a 4π arrangement can greatly enhance

the selection of the desired channel [3–6]. Furthermore, for heavy neutron-deficient compound systems, fission limits the population of high spin states in the residues and this often leads to similar γ-ray multiplicity distributions from evaporation residues and fission events. In this case, charged particle gating becomes very important for selecting the desired channels and for removing the large γ-ray background from fission. We note that charged particle emission from the fission fragments is very low relative to the compound nucleus.

When 4π counting of charged particles is employed, one usually faces the problem of absorption and scattering of the γ rays through rather massive particle detector arrays, which can cause deterioration of the response of the associated Compton suppressed Ge detectors that are typically used in such large arrays, by decreasing the peak-to-total ratio (P/T) of γ detection. While a device capable of particle identification and possibly good energy resolution is required to investigate the interplay between statistical charged particle emission and the feeding of discrete bands [7], these capabilities are not necessary for discrete line spectroscopic experiments. In evaluating what is the best particle detector for a specific task, it is important to keep in

* Corresponding author. Tel. +1 314 935 6504, fax +1 314 935 6184, e-mail dgs@alpha.wustl.edu.

mind the counting rate capabilities of the various possible devices. In spectroscopy experiments, γ-ray energy resolution, statistics and the quality of the Compton suppression are of paramount importance. Thus, for example, we have found that for spectroscopic studies, the advantages of particle identification and energy information provided by the CsI(Tl) detectors of the Dwarf Ball [3] are offset to some extent by a) the substantial increase of background due to scattering of photons in the rather massive Dwarf Ball system, and b) the counting rate limitations (<5000 counts/s) in each element, which limits the event rate because in that device all detectors have equal solid angle. Clearly, the scat-. tering problem can be substantially reduced by minimizing the mass or the atomic number of the charged particle detectors. In this paper a 4π device, which we call the "Microball", is described, which was constructed with the above issues in mind.

In Section 2 we give a description of the detection system, including the design requirements, geometry and characteristics of the Microball, performance simulations, performance tests and results. In Section 3 a schematic description of the new electronics modules constructed for this device is given.

2. Detection system

2.1. Design requirements

The design criteria for a 4π charged particle detection device are based on the physics capabilities that the device will address. In the present case we designed a device that will optimally select exit channels by particle identification for the purpose of detailed spectroscopy with Gammasphere without significant deterioration of the Gammasphere performance. In this case, the reactions of interest are limited to near Coulomb barrier energies and thus only light ions of relatively low energy need to be detected. This choice allowed us to use low mass detectors. On the other hand, if reaction mechanism studies are of interest, one needs to stop more energetic light ions, which requires thicker detectors. Instead of compromising the performance of the Gammasphere by using somewhat thicker detectors for the more energetic particles, we opted to build two such devices. A thin detector device, the *Spectroscopy* Microball, was constructed with minimum possible mass to give optimal channel selection. A thicker detector version, the *Reaction* Microball, allows more energetic particles to be measured. In the latter case certain compromises in absorption and scattering will be made for applications that employ Gammasphere. However, for most anticipated reaction studies with Gammasphere only particle–γ, or particle–γ–γ coincidences will be measured and the absorption losses may not be too severe. The need to use the *Reaction* Microball with Gammasphere limits the projectile energy range for reasonable use of the device to ≤15 MeV/nucleon. The two devices described here have the same geometry and share the same electronics.

We can summarize the detailed design requirements for the Microball as follows:

(i) *Good charged particle identification* (PID). The detectors of the device should provide charged-particle identification capabilities, which are essential in selecting reaction channels.

(ii) *Large solid angle coverage (≃97% of 4π) for good channel identification.* This requirement is important when a weak channel such as (HI,p2n) needs to be selected in the presence of much stronger channels such as (HI,3p). This large coverage can be achieved geometrically, but there are other factors that may reduce further the actual detection efficiency. In principle the device of choice should provide adequate particle identification at all particle energies. However, at large angles for more symmetric reactions and/or lighter compound systems the lowest energy α particles and protons may not be completely distinguished, and this will decrease somewhat the identification efficiency. The importance of large efficiency is apparent, for example, when channels like (HI,3p) or (HI,4p) need to be measured.

(iii) *Small total mass.* This requirement is essential to minimize degradation of the peak-to-total ratio of the Gammasphere Ge detectors. It is imperative for spectroscopic studies, but not as crucial for reaction mechanism studies.

(iv) *Adequate segmentation.* This is important in order to distribute nearly equally the counting rate among the detectors for as many reaction asymmetries in the entrance channel as possible. This will allow the device to keep up with the high event rates of Gammasphere. Decreasing the solid angle of each detector with decreasing angle relative to the beam allows angular distributions of light charged particles to be measured with nearly equal statistical quality for all angles.

(v) *Reasonably good energy resolution.* This requirement permits measurement of particle evaporation spectra with good energy definition below and above the emission barrier.

(vi) *Excellent gain stability with counting rate, temperature and time.* These are very important for obtaining good quality data. Often counting rate dependent shifts may not be possible to correct in the offline analysis, or it may require very time consuming gain shift corrections in order to retain the PID.

(vii) *The device should be small enough to fit inside the Gammasphere scattering chamber.* This is an obvious requirement if the Microball is to be used with Gammasphere. One should keep in mind that other triggering devices might be needed external to the Microball but inside the Gammasphere.

The above diverse requirements limit severely the choice of the detector material and the geometrical design. We have

opted against the choice of Si as the detector material, be-cause such a device would be impractical for high energy particle identification where the (ΔE, E) method must be used, since this is difficult to implement with high solid an-gle coverage. Furthermore, at low energies (for 1–4 MeV α particles) subnanosecond timing must be used for particle identification by time of flight, and this is not possible at all sites where Gammasphere will be implemented.

We have chosen the CsI(Tl) scintillator as the detector material. Using a high thallium concentration, (1200 ppm), it is possible to achieve excellent PID resolution by pulse shape discrimination (PSD). Coupled with a Si photodiode readout of the scintillation light, these detectors satisfy all of the above criteria. CsI(Tl) has two decay components. The first one has a mean decay time $\tau = 0.4$–1.0 μs, the amplitude and fall time of which depends on the particle type detected. The second component has a decay time of 7 μs, which is independent of particle type. These two components can be used to distinguish between particle types by PSD methods. The long 7 μs component presents an important limitation for the CsI(Tl) detectors, because it limits the counting rate that can be achieved without PID deterioration due to pileup. To avoid this limitation we have opted to design the geometry of the Microball in a way that equalizes the counting rate as much as possible among detectors at all angles.

The thickness of the CsI(Tl) scintillator is crucial to the performance of the two devices. The detector thicknesses were chosen on the basis of simulations of the Gammasphere performance coupled with reasonable reaction kinematics calculations. These simulations are described in Section 2.3.

2.2. Geometry and characteristics of the Microball

The geometry and segmentation of the Microball is deter-mined by the counting rate considerations, and the packing limitations associated with the size of the Si photodiodes taking into account the light collection efficiency from the scintillators. We must emphasize that for each reaction stud-ied there is always a best suited geometry. In order to make the device as versatile as possible a compromise solution must be chosen based on a "typical" reaction.

First, the counting rate considerations coupled with the desire to measure adequate particle angular distributions was used to choose an appropriate segmentation for the device. Let us assume for the worst case scenario a reaction that emits on the average 3 charged particles (a fusion reaction near the Coulomb barrier for compound nuclei in the mass 85 region). Assume further an average γ-ray multiplicity of 15 and an event rate that gives 9000 counts/s per Ge detector in the Gammasphere. The geometric coverage of the Ge detectors is $0.5 \cdot 4\pi$ for 110 detectors, while a typical triggering efficiency may be 0.95. Under these conditions the event rate is

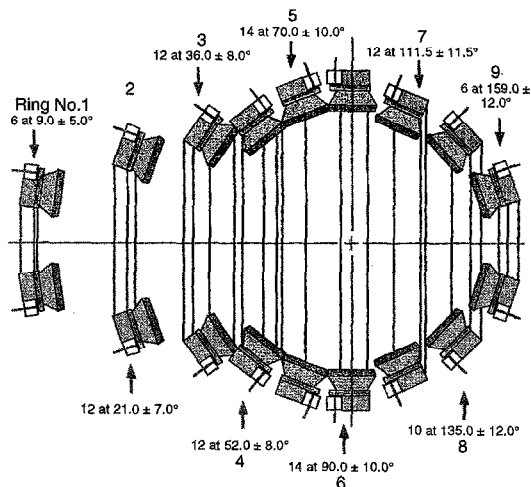$$\text{Event rate} = \frac{9000 \times 110}{15 \times 0.5 \times 0.95} = 1.39 \times 10^5 \text{ events/s}.$$

Fig. 1. Schematic diagram showing a vertical section of the Microball. The number of detectors for each ring is indicated.The azimuthal angle θ and the half angle are also given. The detectors are shown in black facing the target, the light guides are shown as blue trapezoids, the diodes are shown in green, and the supporting Delrin rings in shaded red. The detectors are shown attached to the rings via the gold plated pins (red lines) of the photodiodes.

If we limit the counting rate per CsI(Tl) detector to 4500 counts/s, which is the maximum rate with acceptable pileup fraction (see discussion below), then

$$\text{Number of detectors} = \frac{1.39 \times 10^5 \times 3}{4500 \times 0.97} = 96,$$

where 0.97 is an assumed triggering efficiency.

This number of detectors was selected because it gives a convenient choice of packing the detectors in rings and is also a multiple of 16, thus leading to 6 electronics modules with 16 channels each. This worst case scenario indicates that with 96 detectors the Microball will keep up with the Gammasphere high rates.

A vertical schematic section of the Microball is shown in Fig. 1. There are 9 rings of detectors spanning the angular range between 4.0° and 171° relative to the beam. A close-up photograph of the Microball in the Gammasphere is shown in Fig. 2, while an overview of the Gammasphere with the Microball in place is shown in Fig. 3. The parameters of the Microball are summarized in Table 1. The number of the detectors and their distance from the target in each ring are given in the second and third rows, respectively. The fourth and fifth rows give the polar angles at the center of each ring and the corresponding half angle. A spherical polar coordinate system is used with the beam along the z axis. Rows six and seven give the solid angle for one detector at each ring in msr and the normalized solid angle relative to a detector in the first ring. The next row gives the light guide thickness in mm. The last 6 rows give the average CsI(Tl) thicknesses in each ring for the two devices, as well as the maximum energies of protons and α particles that stop in the detectors.
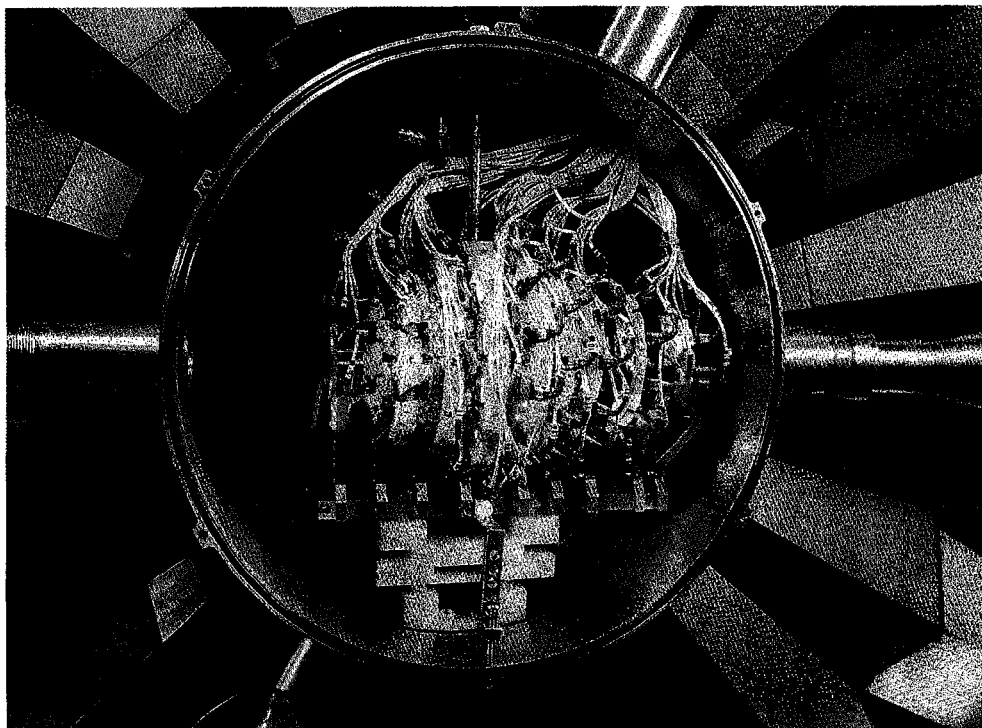
Fig. 2. Close-up photograph of the Microball installed in Gammasphere. The Microball detectors are supported by thin Delrin rings which are held by aluminum legs. The supporting structure allowing 9 degrees of freedom (rotations and translations) is used to align the device to the chamber and the beam axis. The detectors are held by rectangular blocks that hold the two leads of the photodiode. The signal cables are thin shielded coaxial cables (75 Ω) with teflon insulation and connect the diodes to their preamplifiers located outside the vacuum. Ring 6 is located at exactly 90° and it has an opening to allow the target rod to be inserted in position.
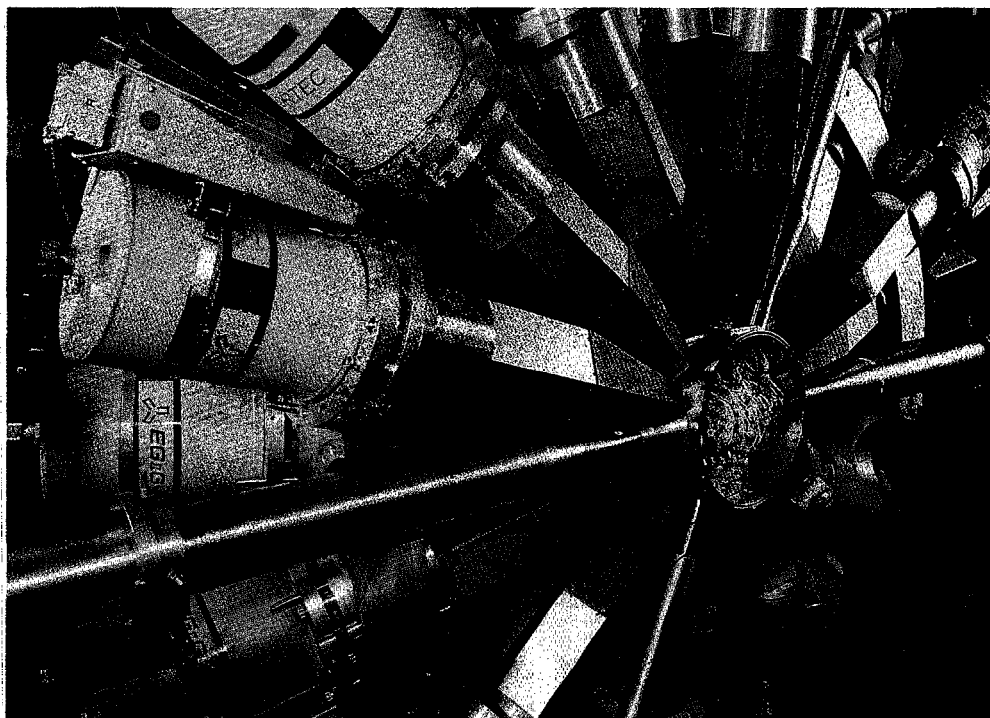

Fig. 3. An overview of one hemisphere of the Gammasphere with the Microball in place. The beam enters from the left.

Table 1
Geometric parameters of the Microball. The maximum proton and α-particle energies that stop in each ring of detectors are also listed.

Quantity	Ring								
	1	2	3	4	5	6	7	8	9
No. of Detectors	6	10	12	12	14	14	12	10	6
Distance [mm]	110	80	60	50	50	50	45	47	50
θ°	9.0	21.0	36.0	52.0	70.0	90.0	111.5	135.0	159.0
Half θ°	5.0	7.0	8.0	8.0	10.0	10.0	11.5	12.0	12.0
$\Delta\Omega$ [msr]	28.2	54.4	85.3	113.2	144.7	154.1	192.1	182.9	154.5
$\Delta\Omega/\Delta\Omega(9^\circ)$	1.0	1.93	3.02	4.01	5.13	5.46	6.81	6.49	5.48
Light guide [mm]	8.0	7.5	6.0	6.0	6.0	7.0	7.0	7.5	8.0
μBall 1, CsI [mm]	2.7	2.4	2.2	1.9	1.6	1.5	1.5	1.3	1.1
p range [MeV]	24.5	22.8	21.7	19.9	17.9	17.3	17.3	15.8	14.3
α range [MeV]	97.0	90.4	85.6	78.7	71.0	68.3	68.3	62.7	56.6
μBall 2, CsI [mm]	9.2	7.2	6.4	6.0	5.6	5.2	4.1	3.6	3.5
p range [MeV]	50.1	43.5	40.6	39.1	37.6	36.0	31.3	29.0	28.6
α range [MeV]	198.6	172.3	161.0	155.1	149.1	142.7	124.1	115.0	113.2

The Microball detectors are planar. Each detector rests with its neighbors because the shapes are cut with compound arcs. This was preferred over a trapezoidal shape because it provides a better packing arrangement without any shadowing of detectors from the neighboring rings. The designed gap between detector elements in each ring was 0.12 mm while the gap between neighboring rings was 0.10 mm. The loss of solid angle due to the designed gaps is approximately 1.8% of 4π, while the space for the target insertion is 0.9% of 4π. The beam entrance and exit openings account for 0.74% of 4π. This gives an overall solid angle coverage of 96.5% of 4π.

The plastic rings that support the detectors are held by legs that move in a rail allowing the placement of each ring at the appropriate distance. The detectors were glued to their UV transparent light guides by Bicron BC-600 epoxy. The light guides were attached firmly to the photodiode by a silicon RTV glue that remains sufficiently soft to allow decoupling from the diode by firmly applying a twisting force. The two diode leads serve to attach each detector to its ring via two plastic parallelepipeds and one supporting screw, making the removal of an individual detector easy. The side surfaces of the detectors were covered with TiO_2 reflecting epoxy. Additional teflon tape was used to protect the active edges of the Si photodiodes. The front surface of each detector was covered by 0.5–0.9 mg/cm^2 Al leaf which is held in place by Pb or Sn absorber foils which were glued on the sides of the light guides. The absorbers were sufficiently thick to stop the elastically scattered heavy-ion beams which typically have a range from 30 to 20 mg/cm^2. Beyond the typical grazing angle the Sn absorbers range from 15 down to 5 mg/cm^2, for the most backward angles. Each absorber is grounded to the supporting Al legs and then to the scattering chamber. This prevents sparking due to charge buildup from the target electrons when intense heavy-ion beams are used.

The scattering chamber consists of a cylindrical portion, 15 cm high, oriented with its axis perpendicular to the beam and in the horizontal plane. Two spherical bowls enclose the

two ends. The chamber is supported by a leg entering from the bottom vertical pentagonal position in Gammasphere and has the 96 Microball signal cables exiting from the opposite pentagonal position. In this way Ge detectors need not be removed to support the chamber and extract the signals. The preamplifier box is located just outside the Gammasphere supporting shell and its lower edge can be seen in Fig. 3. Alignment of the Microball and/or repair of detector elements, mainly connections, is easy. The design of this chamber is fairly simple but due to space constraints we cannot use an external target changer. Instead, we have the capability of mounting two targets on a single frame which can be moved and positioned with Al spacers without breaking the vacuum. The support structure can be seen in Fig. 2.

The target is inserted at an angle of 90° to the beam in the position of one detector in ring 6 (see Fig. 2). The ring was modified to allow insertion of the target frame and support rod. For beam focusing a glass imaging rod 6.5 mm in diameter consisting of optical glass fibers of 0.1 mm diameter is placed at the target position. By making a 90° bend to the rod and placing phosphor on a microscope cover glass at the target position it is possible to view the beam spot through a view port without removing another particle detector.

2.3. Performance simulations

In order to choose the characteristics of the Microball in the best possible way, detailed simulations were carried out with the Monte Carlo code GEANT [8] prior to the construction of the device. The full geometry of Gammasphere was entered in the code GEANT and performance tests for γ-rays of various energies were done. The materials in the vicinity of the Ge detectors had to be accurately included in the simulation in order to obtain realistic values of the peak-to-total ratios as a function of energy.

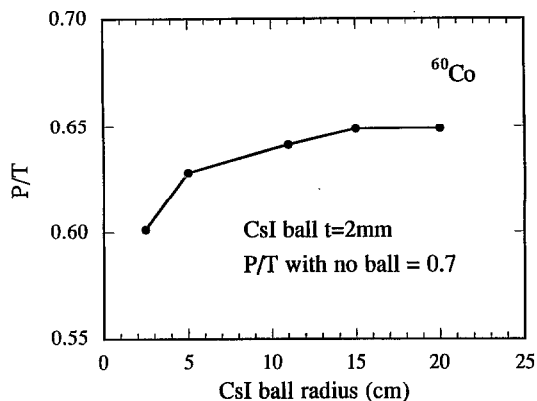The geometry of the Microball was introduced in the code and was assumed to act as an absorber and scatterer. Calcu-

Fig. 4. Peak-to-total ratio of the γ-rays of a Ge detector as a function of the radius of a spherical 2 mm thick CsI(Tl) shell. (Courtesy J.R. Beene, ORNL).

lations with different γ-ray energies were carried out and the results were examined. It was found that a reasonable typical thickness of ≈ 1.5 mm for the CsI(Tl) detectors would be adequate for the spectroscopy version of the Microball.

Fig. 4 shows the results of a simulation of the peak-to-total ratio (P/T) of ^{60}Co γ rays as a function of the radius of a shell of 2 mm thick CsI(Tl). The Compton suppressed Ge detector had a (P/T) of 0.7. Clearly, one should make the device as large as possible, but above about a 7 cm radius further improvements are marginal. From this simulation and from the limitations due to the size of the photodiodes and/or the size of the scattering chamber coupled with the efficiency of light collection we have chosen the radius to the detector back side from the target center to vary from 4.5 to 11.0 cm for rings 9 to 1.

In Table 2 we give the results of a simulation for the Ge detectors of Gammasphere to 300, 500, 800, 1200, 1500 and 2000 keV γ rays for the following situations: a) A Ge detector in Gammasphere without Compton suppression, b) a Ge detector in the Gammasphere with Compton suppression only by its own BGO shield, and c) a Ge detector in Gammasphere suppressed with its own BGO plus any BGO from the neighboring detectors. Also are given the situations as in a), b), and c), but with the Microball in place. The average peak efficiency loss due to the insertion of the Microball is also given. The reduction of the P/T ratio for the three conditions and the six energies are also given.

The reduction of performance due to the assembling of the Gammasphere compared to a stand-alone Ge detector is not shown here, but is found to be larger than that caused by the Microball. In summary the reduction of the P/T ratio due to the Microball is approximately 0.91 ± 0.01. This reduction is indeed small, especially when one realizes that additional reduction of the P/T ratio occurs when high multiplicity events are considered. These produce significant coincidence summing (~ 10–15% depending on M_γ) and additional scattering.

2.4. Performance and design tests

Experimental tests were made for the purpose of selecting and fine tuning the performance characteristics of the Microball detectors and their associated electronics. These tests were carried out with alpha sources (^{232}U, ^{249}Cf and ^{252}Cf). They included a) the energy resolution, b) the counting rate stability, c) the particle identification resolution by pulse shape discrimination, and d) temperature stability. The energy resolution is intimately coupled to the geometry of the detector assembly and the quality and design features of the associated electronics. The counting rate stability and in part the PID resolution depend on the electronics, while the temperature stability is a function of the crystal and the electronics. These factors are discussed below.

2.4.1. Detector geometry and energy resolution

We have carried out a series of tests aimed to determine the importance of the geometry of the light guides of the energy resolution of the Microball detectors. The geometry of the entire Microball was programmed in the computer so that the distance of the rings from the target and the thickness and shape of the light guides could be easily calculated and varied.

Remembering that the detectors have the shape of portion of cone, and that their area is approximately 2 to 4 times that of the 10.0×10.0 mm^2 Si diode, we would need a matching light guide having an arc shape in one end and square at the other. For the purposes of these tests we approximated the detectors shapes with trapezoids of equal area. We used a highly doped CsI(Tl) with 1200 ppm in Tl, which was found to give optimal PID resolution[9] and prepared matching light guides. To insure that the tests reflect the effect of the geometry, we scanned the crystals in two dimensions with a collimated α source and at the same time measured the energy resolution. We found that the thickness and the shape of the light guide strongly influenced the uniformity of response. With the chosen light guide shapes we achieved a uniformity better than 0.7% across the face of the detector and obtained an energy resolution of 2.7% for 8.78 MeV α's. This is indeed two times better than that achieved with the Dwarf Ball detectors, where photomultipliers are used. Taking into account the fact that the Si photodiodes have a quantum efficiency of $\simeq 80\%$ as compared to $\simeq 20\%$ for the phototubes, the improved energy resolution is in accord with the photon statistics, indicating that the losses due to geometry are similar for the two detector arrangements. The thickness of the light guides given in Table 1 were selected to optimize the resolution.

Fig. 5 shows a typical spectrum of α particles measured with a detector in ring 2 using a ^{232}U α source. The detector front was only covered with aluminized (0.29 mg/cm^2) Mylar. The spectrum was taken with the appropriate Microball electronics. The nonlinear response of the CsI(Tl) is clearly seen from the energies and channel numbers given.

Table 2
GEANT simulation of the single γ-ray response of the Gammasphere for six γ-ray energies. The numbers given are the Peak-to-Total ratios in a Ge detector and are averages of the 3 geometries of BGO shields. The statistical uncertainties in all the numbers are given by the last two digits and correspond to the last two significant figures.

| Config. | E_γ [keV] | | | | | |
	300	500	800	1200	1500	2000
(P/T) Gammasphere						
Unsuppressed	0.723 08	0.509 06	0.374 05	0.285 04	0.255 04	0.234 04
Own BGO shield	0.882 11	0.795 11	0.692 11	0.568 10	0.525 09	0.476 09
Own + neighbors's	0.886 11	0.829 11	0.764 12	0.659 11	0.612 11	0.565 11
(P/T) Gammasphere + μBall						
Unsuppressed	0.662 08	0.451 06	0.348 05	0.277 04	0.252 04	0.236 04
Own BGO shield	0.808 11	0.723 10	0.637 10	0.541 09	0.510 09	0.475 09
Own + neighbors's	0.812 11	0.751 11	0.701 11	0.620 11	0.582 11	0.557 10
Peak Eff. Loss	0.817 08	0.854 08	0.936 09	0.951 10	0.977 10	0.973 10
P/T Red. by μBall						
Unsuppressed	0.916 13	0.886 15	0.930 18	0.972 20	0.988 22	1.008 24
Own BGO shield	0.916 13	0.909 19	0.920 21	0.952 24	0.971 24	0.998 25
Own + neighbors's	0.916 13	0.906 19	0.917 21	0.945 24	0.951 24	0.986 25

The peak labelled 5.32 MeV is a composite of 4 lines. At low energies, the broad structure labelled β^- is the composite of several beta groups with an average end point energy of ~2.4 MeV. The energy resolution (FWHM) at 8.78 MeV is given as 240 keV. When the necessary absorbers for in beam work are in place the energy resolution for α lines from the source deteriorates according to the absorber thickness.

We have measured the noise and energy resolution as a function of cable length between the photodiode and the preamplifier. We tested 2 cables, an RG174 and a much thinner shielded cable with the same capacitance (1.0 pF/cm) per unit length. We found that for up to 1.8 m the resolution deteriorates slowly at a rate of $\approx$ (0.6%)/m independent of the cable thickness. We have chosen lower capacitance (0.6 pF/cm) thin shielded cables 1.2 m long for all the detectors. These are sufficiently long to allow placement of the preamplifiers outside the Gammasphere shell. The loss

Fig. 5. Energy spectrum from a ^{232}U α source. The detector was one in ring 2 and it was covered in front by 0.29 mg/cm² aluminized Mylar. The peaks are labelled in MeV. The structure at low energies labelled β^- is the sum of several groups with an average end point of about 2.4 MeV. The nonlinearity of the response for α particles at these energies is clearly seen.The energy resolution at the 8.78 MeV α peak corresponds to a FWHM of 240 keV.

of resolution with cable length was somewhat less for the lower capacitance cable.

2.4.2. Counting rate stability

We have measured the counting rate stability with a 4.5 μCi ^{249}Cf α source that could be moved remotely to vary the rate. The stability as a function of rate depends entirely on the pole-zero compensation and base line restoration employed in the slow shaper of the electronics system. Several schemes were tried. The adopted one gave an impressive stability of $\leq$0.5% between rates of 500 counts/s and 12 000 counts/s. No gain variation was observed below 5000 counts/s. For higher average energies the gain shift may be somewhat larger, but over the range of counting rates for which the device is designed ($\leq$4500 counts/s) no significant gain shifts are observed.

2.4.3. Timing resolution

The timing resolution of CsI(Tl) is limited due to the slow rise time (15 ns) and the small amplitudes. With the appreciable integration introduced in the preamplifier, a compromise has to be reached between timing resolution and energy threshold. We have chosen a rather long crossing time of 600 ns for the constant fraction discriminator. This choice was motivated by the competing features of low threshold and the ability of the system to utilize cross-over time as a second simultaneous method for particle identification by pulse shape discrimination.

We measured the timing resolution of the CsI(Tl) detectors using a ^{249}Cf source that gives a 5.8 MeV α in coincidence with a 388 keV γ ray. A fast CsF detector was used for the fast channel. We obtained a FWHM of 55 ns. This was found to improve to about 20 ns for more energetic particles of about 18 MeV and still provide a triggering capability down to ~200 keV α particles without noise.
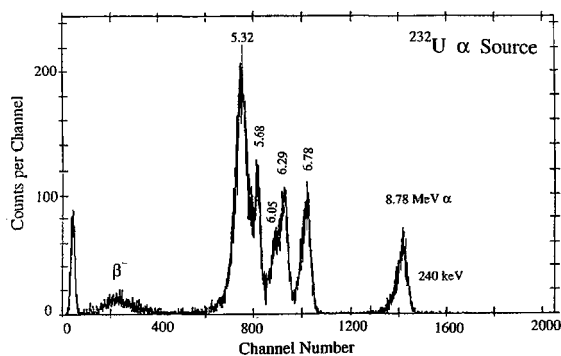
2.4.4. PID resolution by pulse-shape discrimination

Good PID resolution is crucial to the performance of the Microball. Therefore we have carried out extensive tests in order to obtain the best possible resolution. The PID resolution is critically dependent on the preamplifier and shaper used. A detailed description of the electronics is given in Section 3.1. Here we summarize the experimental results. The charge-sensitive preamplifier employed integrates considerably the photodiode signals and produces pulses with a rise time of $\sim 1\mu s$ and a decay time of $\sim 300\mu s$. A low and high frequency filtering two-stage shaper is employed to recover the two components of the CsI(Tl). An aperiodic pulse with the shape proportional to $x^4 e^{-4x}$ where $x = t/\tau_0$ is used. Tests with τ_0 values of 1.3 and 1.8 μs were made. The pulse shapes were simulated using a computer code that gives the output pulse of the actual shaper circuit for any input. Using input pulses with exponential decay times of 0.7 μs and 7.0 μs, we obtained the simulated pulse shapes that guide us as to where to place the gates for integrating the charge for the two components. The simulated pulse shapes corresponding to $\tau_0 = 1.3\mu s$ give a peaking time of 2.8 μs for the 0.7 μs component and $\sim 6\mu s$ for the 7.0 μs component that shows a long tail. Remembering that the 7.0 μs component carries only a fraction ($\sim 1/2$) of the light of the shorter component we have used these relative intensities in the simulations. We conclude that the best place for the gates are near the peak and at $\sim 12\mu s$, respectively. However, the long tail produces pileup. A good compromise is found by using the pole-zero compensation to reduce the tail and then move the tail gate up to about 9 μs.

We have been fine tuning the electronics to obtain the best PID resolution by measuring two-dimensional distributions using an α source of ^{232}U which provides several α peaks with energies of 5.32, 5.684, 6.051, 6.287, 6.777, and 8.785 MeV, as well as β^- groups with end point energies of ~ 2.4 MeV. These α and β particles can be easily identified on the bench top by pulse shape discrimination (PSD).

Typical PID resolutions from a ^{232}U source are shown in Fig. 6 where in the scatter plot the abscissa is the E component (0.7 μs, FAST, a 1.0 μs gate reaching the peak of the signal) and the ordinate is the slow component (a 10 ns gate at 9.0 μs). The α particle separation from the ($\beta^- + \gamma$) pulses is clearly seen down to very low energies. In the maps of Fig. 6 protons are expected to be located half between the α's and the electrons, it is clearly seen that the proton-α separation at energies from $E_\alpha \geq 2.0$ MeV and $E_p \geq 1.0$ MeV is achieved. This indicates that the spectroscopy version of the Microball should work as expected down to very low energies.

In Fig. 6b the detector viewed α particles and fission fragments from a ^{252}Cf source and from a ^{232}U source. The direct identification of the fission fragments is also seen. Note that the CsI(Tl) scintillator was covered with 290 $\mu g/cm^2$ aluminized Mylar that attenuates the energy of the fission fragment considerably, but the largest reduction in pulse
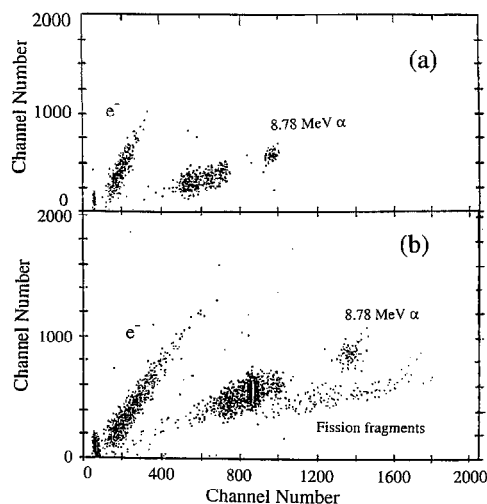

Fig. 6. Scatter plot showing the PID resolution by pulse shape discrimination. (a) shows the separation of α particles and electrons or γ-rays from a source of ^{232}U. A prototype preamplifier and electronics module were used. (b) Separation by PSD of electrons, α particles and fission fragments from a ^{252}Cf source is seen. The detector was covered by 0.29 mg/cm^2 aluminized Mylar.

height comes from the strong light quenching in the CsI(Tl) from the high ionization density. For in-beam applications the necessary absorbers for stopping the elastically scattered beam and the target electrons and x-rays, completely stop the fission fragments. For the Microball detectors to trigger on fission fragments one must remove the absorbers for angles larger than grazing and decrease the beam intensity considerably. This would make spectroscopic studies with a fission veto impractical.

2.4.5. Temperature stability

The detector system was checked for stability of gain and overall performance against variation in temperature. With the preamplifiers located outside the scattering chamber the Microball itself remains at the ambient temperature. The only variation in gain is known to originate from changes in light output of the CsI(Tl) scintillators [10]. A small variation in gain results from the change in operating temperature of the preamplifiers. No change in gain could be observed after an hour from powering up the system.

2.5. In-beam performance of the Microball

2.5.1. Particle identification by pulse-shape discrimination

Based on the above tests, the design and construction of the Microball was completed and used in a number of experiments. While for the spectroscopic studies it may be sufficient to separate protons and α particles, for the thicker device for reaction mechanism studies it is important to separate p,d,t, ^{3}He, α, Li, Be and perhaps heavier ions.

The particle identification capabilities of the spectroscopy Microball via pulse shape discrimination is illustrated in
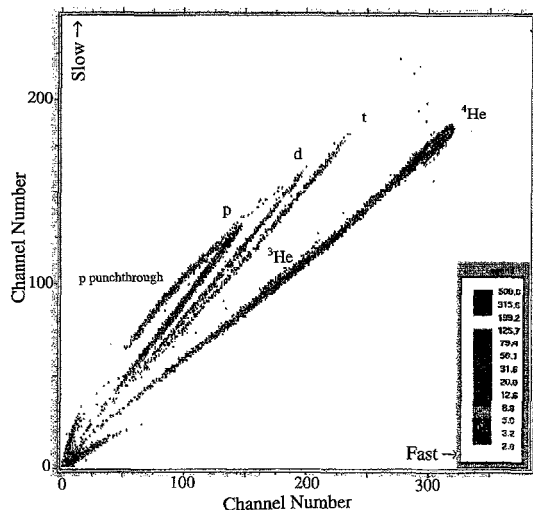
Fig. 7. Color scatter plot showing the PID resolution by pulse-shape discrimination using a 1.9 mm detector. The reaction was 48 MeV ^{4}He on ^{197}Au. The p, d ,t separation is clearly seen. The separation of α particles from the hydrogen isotopes is apparent for all energies down to very low energy. The proton punchthrough energy here is 19.9 MeV. The data were from the calibration run of an experiment in Gammasphere.
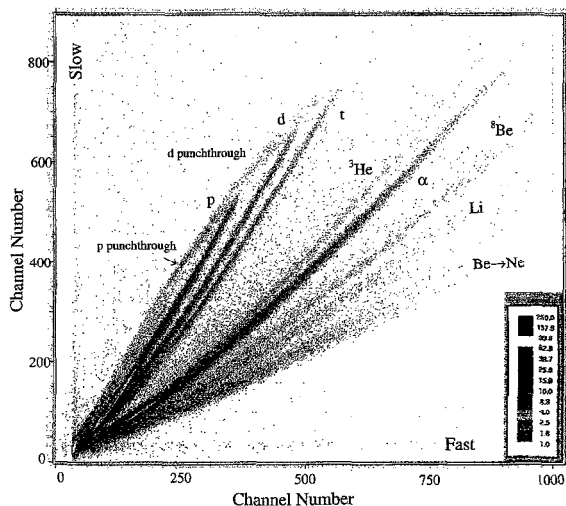

Fig. 8. Color scatter plot showing the PID resolution by pulse shape discrimination using a 6.4 mm detector. The reaction was 300 MeV ^{20}Ne on ^{93}Nb. The p, d, t separation is clearly seen. Separation of ^{3}He from α particles down to reasonably low energies is seen. The first line below the α line is the 2α line from the ^{8}Be breakup. The next line shows the Li ions detected and the lowest one is the group of all heavier ions from B to Ne. The proton punchthrough energy here is 40.6 MeV. Our prototype preamplifier and a complete channel of the new electronics was used to process the signals.

Fig. 7 where a color scatter plot of data collected at 52° with a 1.9 mm CsI(Tl) detector using the reaction of 48 MeV α particles on ^{197}Au is shown. The counting rate in this measurement was limited to $\leq$ 1000 counts/s. The excellent separation of the hydrogen isotopes (p,d,t) from each other and the α particles is clearly seen. Small amounts of ^{3}He are also seen. When the energies of p,d, and t particles exceed the ranges in the 1.9 mm CsI(Tl) they appear as punch-throughs as indicated in the figure. In this case the proton range is 19.9 MeV. The punch-through energies of these light ions can be used as additional energy calibration points.

Here we must emphasize that for nuclear spectroscopic studies with the Microball and Gammasphere the demand for maximum statistics requires high counting rates in each of the particle detectors ($\sim$4000 counts/s). Under these conditions the PID resolution deteriorates somewhat. The deuterons are still resolved from the protons for most of the forward detectors, but at large angles the low d yields do not allow separation from the protons. For all energies, however, the protons are well separated from the α particles.

As a test of the performance of the "Reaction" Microball we used a rather energetic reaction of 300 MeV ^{20}Ne on ^{93}Nb. This reaction produced high energy p,d,t, ^{3}He, α, Li, Be ions at the forward angles. As expected the light ions had energies that exceeded the range in the 6.4 mm detectors. Consequently the light ions punched through but still were well identified. In Fig. 8 we show a color scatter plot from a 6.4 mm CsI(Tl) detector at 21° to the beam. Again excellent PID resolution is seen. Now the proton punch-through energy is 40.6 MeV and that of the deuterons 54 MeV. Reasonable ^{3}He–α separation is seen. One can clearly see the ^{8}Be breakup line into two α particles (first line below the

α line). The Li and the remaining heavier species are also clearly resolved.

2.5.2. Particle identification by pulse-shape discrimination and zero crossing time

It was mentioned earlier that reasonable particle identification can be obtained from the cross over time of the differentiated fast signal of the constant fraction discriminator. In this case as reference time we take the RF time of the cyclotron. In the present example we used the reaction of 180 MeV ^{35}Cl on ^{105}Pd. In Fig. 9a we show a color scatter plot of the Fast component (energy) vs. the zero crossing time (ZCT) minus the RF for a typical detector at 36° and a 2.2 mm thickness, operating at a counting rate of 4000 counts/s. It is seen that the α particles have significantly better timing resolution, partly due to their higher energies. Note that time flows as indicated, with the α particles having smaller ZCT.

The particle identification resolution using the ZCT is not as good as that from pulse shape discrimination using the R = Slow/Fast ratio method. We demonstrate this for the same reaction and detector in Fig. 9b, where a color map of the Fast component vs. the ratio R. The optimal separation of the particles over a large dynamic range in energy is obtained by combining the two procedures illustrated in Figs. 9a and 9b. This is shown in Fig. 9c as a color plot of the ZCT vs. R for the same reaction. By placing curved masks in the latter map it is possible to obtain the best separation of the particles and to reject a larger fraction of the random coincidences.

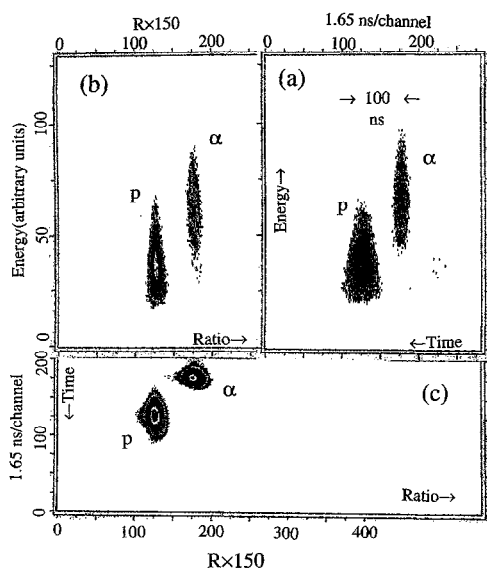It should be noted that in some cases where base line in-

Fig. 9. (a) Color scatter plot of the linearized Fast component vs. the zero-crossing time minus the RF (*ZCT*). The data are from a 36° detector from the reaction of 180 MeV ^{35}Cl on ^{105}Pd. The time flows to the left and the proton to α separation is 100 ns. (b) Color scatter plot of the linearized Fast component vs. the ratio R = Slow/Fast from the same detector and reaction as in (a). In (c) a color scatter plot of the ratio R vs. (*ZCT*) is shown for data from (a) and (b). Here the data go down to a few percent of the peak for the protons and α particles.
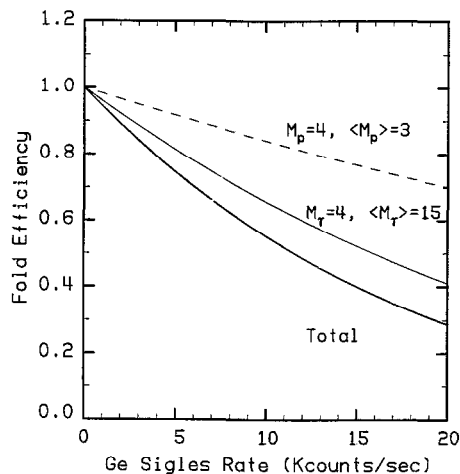

Fig. 10. Fold efficiency or losses due to pileup in the Microball and Gammasphere as a function of the Ge singles rate in the Ge detectors. The dashed and thin lines give the pileup losses in the Microball and Gammasphere, respectively. The thick line is the product of the two (see text for details).

stabilities are experienced (usually due to failure in the base line restorer) the resolution by the ratio method deteriorates more rapidly than the ZCT one. In this case the combined approach provides substantially superior separation.

2.5.3. Pileup losses

For most spectroscopic applications where high counting rates are employed it is important to estimate the losses due

to pileup in the Ge detectors and the Microball. Let F_p and F_γ be the fractions giving the pileup for particles and γ rays, respectively. Then the overall pileup loss is given by $F = F_\gamma F_p$, such that:

$$F_\gamma = (1 - \tau_\gamma R_\gamma)^{f_\gamma}, \quad F_p = (1 - \tau_p R_p)^{f_p}, \quad (1)$$

where τ_γ and τ_p are the dead times for γ rays and particles, respectively. Presently, reasonable values for τ_γ and τ_p are 10 and 9.5 μs, respectively. The quantities f_γ and f_p are the γ-ray and charged particle folds for the channel of interest, respectively. Using Eq. (1) we can calculate the typical pileup losses for the Gammasphere and the Microball as a function of the "singles" γ-ray rate assuming that the particle rate in each Microball detector, R_p, is given by

$$R_p = R_\gamma \frac{\langle M_p \rangle N_\gamma \epsilon_p}{\langle M_\gamma \rangle N_p \epsilon_\gamma \Omega_\gamma}, \quad (2)$$

where $\langle M_p \rangle$ and $\langle M_\gamma \rangle$ are the average particle and γ-ray multiplicities for the reaction at hand, N_γ and N_p are the number of Gammasphere and Microball detectors (110 and 96), respectively, ϵ_γ and ϵ_p are the respective triggering efficiencies of each detector (assumed to be 0.95 and 0.97) and Ω_γ is the geometric efficiency of all the Ge detectors in Gammasphere taken to be 0.5. In Fig. 10 we show the results of such a calculation using the values of 3 and 15 for $\langle M_p \rangle$ and $\langle M_\gamma \rangle$, respectively. The dashed curve gives the fold efficiency (the pileup loss is the difference from unity) for the Microball, the thin solid line gives the fold efficiency for fourfold events in Gammasphere and the thick solid line the total efficiency. We see that for a typical rate of $R_\gamma = 10\,000$ counts/s $f_\gamma = 4$, and $f_p = 4$ the F_γ, F_p and F values are 0.656, 0.757 and 0.497, which correspond to losses of 34.4, 24.3, and 50.3%, respectively. The calculated γ-ray pileup losses shift the events to the lower fold. For the particles they lead to a loss of the events due to mis-identification of the particles. The redistribution of the (HI,4p) channel counts to other lower proton number channels will be addressed below. In the above calculations losses due to detectors removed from the Microball have been ignored.

2.5.4. Channel selection capabilities

The capability of the Microball to select exit channels or groups of them depends critically on the reaction employed, its efficiency for detecting particles, and in the case of channels with several emitted charged particles, on their number.

For a typical reaction with each detector counting at 4000 counts/s the fractional pileup losses are 0.040 which is slightly larger than losses due to geometrical coverage of the Microball which are 0.035. There is an additional geometrical loss of 0.040 due to shadowing of particles by the present target frames (opening diameter of 13 mm and thickness of 0.5 mm). The latter can be reduced to 0.02 if thinner target frames are used. An overall particle detection efficiency of 0.885 is then expected. The measured efficiency for proton
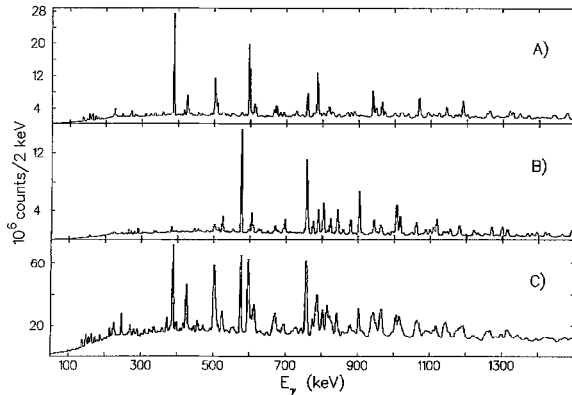
Fig. 11. (a) Low energy part of the spectrum of the γ rays from the α2p exit channel gated by the Microball from the reaction of 130 MeV ^{28}Si on ^{58}Ni. (b) Same as in (a) but for the 4p gate. (c) Spectrum from the same reaction but without any particle gating.

and α detection from the reaction of 230 MeV ^{51}V on ^{100}Mo was found to be 0.88.

This overall particle detection efficiency determines the channel detection efficiency of the device. Thus for the reactions of 130 MeV ^{28}Si on ^{58}Ni, the 4p and α2p exit channels may be expected to be detected with an efficiency of $0.89^4 = 0.63$ and $0.89^3 = 0.70$, respectively. However, for a reaction like the latter one at the most backward angles the reaction kinematics and the absorbers present cause the loss of some of the sub-barrier particles and this reduces the expected single particle efficiency to 0.87.

In Figs. 11a and 11b we show the low energy part of the γ-ray spectrum from the 4p and α2p channels from the reaction of 130 MeV ^{28}Si on ^{58}Ni. It is clearly seen that the γ-ray spectra are completely different. Furthermore, the peak-to-background ratio in these spectra is substantially improved over that in the ungated spectrum, which is shown for comparison in Fig. 11c. For the 4p exit channel approximately 43% of the counts are expected to be distributed among the 3p, 2p, 1p and no particles gates. The distribution of counts among these channels can be in principle calculated from the combinatorial equations. However, this is complicated by the kinematical focusing of the particles and the varying solid angle in the rings.

For purposes of spectroscopy it is important to recognize that for each reaction there is a distribution of cross sections in the various channels. If the channel of interest is one emitting many charged particles, then most likely the cross sections for channels with additional particles will be small and one need not to be concerned with misplaced channels. For example, in the latter reaction the 4p channel will have very few or no counts from the 5p channel. However, if the 1p2n channel is of interest, then significant contributions from the 2p, 3p and 4p channels will be present. In such a case these contributions can be estimated from the line intensities in spectra or matrices from these channels and then subtracted. This works well with E_γ–E_γ matrices but

great care has to be exercised if background cubes are to be subtracted.

The channel selection that is provided by the Microball in general improves the peak-to-background ratio in a particle-channel gate by the inverse of the fraction of the cross section of that channel in the reaction and this in turn improves the resolving power of Gammasphere. In order to demonstrate the increased detection sensitivity by channel selection we show in Figs. 12a and 12b spectra doubly gated using all the combinations of double gates on a superdeformed band in ^{80}Sr from an ungated and an α2p gated E_γ–E_γ–E_γ cube, respectively. No underlying γ background was subtracted. The decrease in the background due to channel gating is clearly seen. As a result of this an additional transition at 2859 keV is clearly seen.

2.5.5. Recoil correction procedures

There is a further significant improvement that the Microball can provide for spectroscopy mainly in the lighter reaction systems. This is the improvement in energy resolution of the Ge detectors for in-beam spectra that comes from a modified Doppler shift correction to take into account the residue recoil direction.

The γ-ray energy resolution in heavy-ion induced fusion reaction is determined essentially by three factors. The first is Doppler broadening due to the finite size of the Ge detectors. For a given set of Ge detectors in an array like Gammasphere this is a fixed contribution. The second one is associated with the Doppler broadening from the slowing down of the recoils in the target. This can be minimized by making the target as thin as reasonable or using a stack of thin targets. However, for very fast transitions as is the case of superdeformed nuclei, there is still a residual broadening due to slowing down in the thin target [11]. We shall come back to this issue shortly. The third one comes from the Doppler broadening associated with the opening angle of the recoil cone. Normally for (HI,xn) reactions not much can be done to improve on the recoil cone. However, for reactions involving a significant number of charged particles a detection of the latter can be used to determine event-by-event an improved recoil cone. For the case where the reaction channel of interest involves only charged particles (we term these *"the total spectroscopy"* channels) the determination of the recoil direction can be complete.

For multidetector systems such as Gammasphere the gain matching is done in a way that includes an overall Doppler shift correction. This was done in the spectra shown in Figs. 11 and 12a and 12b from the reactions of 130 MeV ^{28}Si on ^{58}Ni. In order to properly correct for the recoil direction the energies and momenta of the emitted charged particles must be determined event by event in the center of mass system. From these the recoil momentum and its direction in the laboratory system can be found. This new direction is then used to define the emission angle for each Ge detector relative to the recoil. A comparison showing the improvement in resolution can be seen in Fig. 13. The reaction was
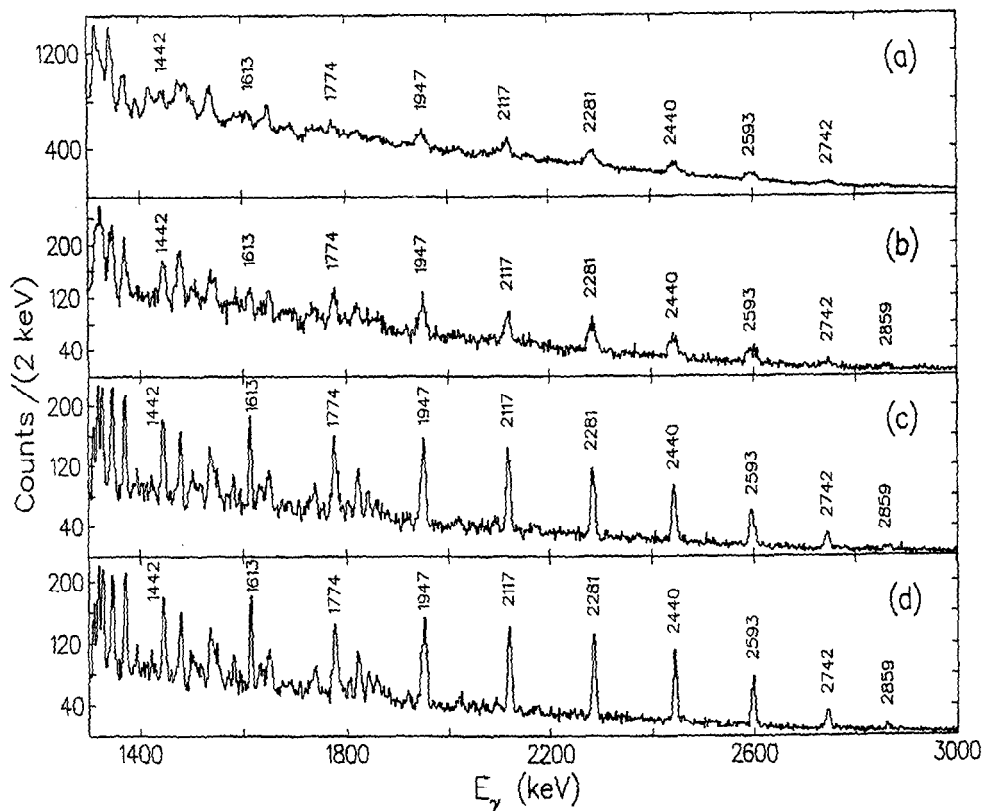
Fig. 12. Gamma-ray spectra of the yrast superdeformed band in ^{80}Sr from the reaction of 130 MeV ^{28}Si on ^{58}Ni. (a) Spectrum from all the Doppler-corrected double gates of γ rays from a cube without any channel selection. (b) Same as in (a) but from a cube that have been gated on the α2p particle channel. The improvement in the peak to background is apparent. (c) Same as in (b) but the Doppler correction from the particle determined recoil direction has been applied. The resolution at 2593 keV improves from 30 to 10 keV FWHM. (d) Same as in (c) but now an γ-ray energy dependent residual Doppler correction taking into account the lifetime of the transitions has been applied. The resolution at 2593 keV improves further from 10 keV to 7 keV FWHM.

128 MeV ^{29}Si on ^{58}Ni producing ^{81}Sr by the α2p channel. The resolution at ~950 keV improves from 11.5 to 4.0 keV, FWHM. For other exit channels in the same reaction that do not involve α particles the improvement in resolution is smaller. Thus, for the 4p and 3p channel the FWHM at 1000 keV improves by a factor of 1.7 and 1.4, respectively, with the final resolution being at ~4.0 keV.

The increased sensitivity due to the Doppler shift correction relative to the recoil direction for the identification of SD bands is shown in Fig. 12c. When the residual Doppler correction due to the slowing down in the thin target is applied, the resolution further improves as can be seen in Fig. 12d.

2.5.6. Energy calibration procedures

The non-linear nature of the light output of CsI(Tl) as a function of Z and energy of the impinging ion complicates the energy calibration of the Microball. A detailed account of the Z and energy dependence of the light output for CsI(Tl) for ions from Z = 1–23 and energies up to ~19 MeV/nucleon has been given by Stracener et al. [3] for the detectors of a similar 4π device, The Dwarf Ball and Wall.

For purposes of fusion reactions near the entrance channel Coulomb barrier, where most of the spectroscopic applications of the Microball are made, we only need to be concerned with energies of protons and α particles that stop in the CsI(Tl) detectors as given in Table 1. For these energies the p,d,t response may be taken as linear. However, for α particles significant nonlinearities are present particularly at low energies (see Fig. 5).

We have measured the light output for α particles from 2.0–8.8 MeV using α sources. We have found that the expression given by Eq. (8) in Ref. [3] well represents the response of the scintillators in the Microball. Presently we employ this equation in the form

$$E_\alpha = apx + b\ln(1 + cpx), \tag{3}$$

where x is the number of channels above the ADC pedestal, p is an adjustable parameter and a, b, and c are constants having the values of 5.980, 0.9800 and 14.00, respectively. These were determined at an arbitrary reference energy of 8.63 MeV α energy. If the value of $px = 1$ is used in Eq. (3) then one finds $E_\alpha = 8.633$ MeV, which is the reference value.
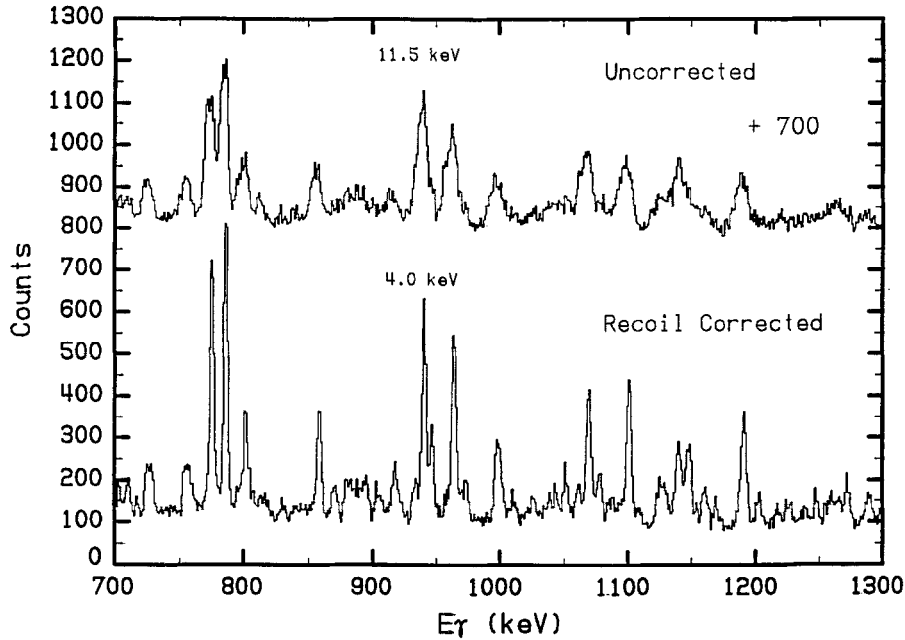
Fig. 13. Gamma spectra from the reaction of 128 MeV ^{29}Si on ^{58}Ni. The spectra have been gated on the $\alpha2p$ channel. The upper spectrum is the uncorrected one with its zero increased to 700 counts for clarity. The lower spectrum is the same but with the Doppler correction relative to the recoil direction. The resolution in this energy region improves by about a factor of three.

The procedure for calibrating all 95 detectors of the Microball consists of using a cocktail beam of 12.00, 24.00 and 48.00 MeV p, d, and α particles from the LBNL 88" Cyclotron. These beams are elastically scattered on ^{197}Au and elastically and inelastically scattered on ^{12}C. In addition, an α source with the 6.051 and 8.785 MeV lines is used for the backward detectors. The proton scattering on ^{12}C produces two peaks (elastic and first excited state of ^{12}C) for all but the first ring of detectors. The elastic scattering of d supplements the p data with an additional high energy point for the forward detectors. By obtaining a proton calibration with 2 or more points allows us to determine accurate pedestal values (channels for zero energy). Only one α calibration point is sufficient to determine the coefficient p in Eq. (3). From such a calibration we determined the internal consistency by calculating the values of the α particle energy that corresponds to 10.0 MeV protons and found an average value of 12.0 MeV with a standard deviation of 2.6% among the 95 detectors.

2.5.7. Performance of Gammasphere with and without the Microball

There are two important properties of the Ge spectra in Gammasphere that are affected when the Microball is inserted in the scattering chamber. These are the peak efficiency and the peak-to-total ratio (P/T) as a function of γ-ray energy. These quantities were calculated in the GEANT simulations shown in Table 2. We have measured the reduction of the peak efficiency due to the insertion of the Microball and found substantial loss of efficiency only below

200 keV. The values in Table 2 for the peak efficiency are in reasonable agreement with experiment.

We have also measured the (P/T) ratio for the ^{60}Co transitions and for 56 Ge detectors we found 0.57 ± 0.01 without the Microball and 0.52 ±0.01 with it. This correspond to a 0.91 ± 0.02 reduction factor. The GEANT simulation for 1200 keV gives 0.95 ± 0.02 for this reduction in (P/T). The calculated value of 0.568 ± 0.010 for (P/T) without the Microball is in good agreement with experiment, but the value of 0.541 ± 0.009 is somewhat higher than the experimental value. This may be due to the fact that some complexities in the Microball assembly such as the signal cables, supporting structures, etc. have not been properly entered in the GEANT geometry. It is interesting to point out that the GEANT simulations suggest that the deterioration of the (P/T) values increases with decreasing energy (see Table 2).

Further details on simulations of other more specific features of the Gammasphere system with and without the Microball will be addressed in a separate publication [12].

3. Signal processing and readout

3.1. Electronics

The electronics system for the Microball consists of four physically separate components. Three of these are grouped in six banks of 16 channels each. They include a) the preamplifiers, b) the integrated electronics modules, and c) the digitization and readout system. The fourth involves the

setup for the gating logic. These four components of the system are described briefly below. The thresholds and gains of the Microball detectors are adjusted by computer control. The details of the Gammasphere acquisition and control system will not be discussed in detail here.

3.1.1. The preamplifiers

The preamplifiers are single board modules with dimensions 2.5 × 5.0 cm that plug in groups of 16 into 6 power distribution boards. These are arranged to form a hexagonal prism that can fit into a cylindrical metal shield with 16 cm diameter, 20 cm long. This shield is directly connected to a vacuum feed-through plate. This plate is directly connected via a vacuum tube to the scattering chamber. This arrangement places the preamplifiers at about 120 cm from the Microball detectors and outside Gammasphere supporting frame structure.

These preamplifiers are charge sensitive [13] and include significant integration to optimize the signal to noise ratio. The output pulses have a rise time of about 600 ns and a decay time of 300 μs.

3.1.2. Integrated electronics modules

We have decided to combine all the functions of 16 detector channels in a one quadruple width CAMAC module. CMOS technology was used. The details of the design of this system will be reported elsewhere [14]. These modules were designed and fabricated at Washington University. A block diagram of the functions in the module is shown in Fig. 14.

For each channel the module incorporates:

(i) Pole-zero compensation. This is important for adjusting the tail of the pulse to minimize pileup.

(ii) Base line restoration for gain stabilization against counting rate variations.

(iii) A fast shaper (peaking time 600 ns) and a differentiation used to produce a Nowlin type constant fraction discriminator output [15]. The peaking time had to be slowed down considerably in order to allow triggering to low energies without excessive noise. The discriminator is cleared after a selectable period of time up to 20 μs. This should be set to exceed the period from the beginning of the fast discriminator to the end of the tail gate.

(iv) An OR circuit for the 16 channels of the CFD output is provided on a single LEMO connector. Its width is nominally set to 100 ns.

(v) A multiplicity output on a LEMO connector is provided. Its output level is adjustable and is set at 50 mV per fold.

(vi) A two-stage aperiodic slow shaper. It is used to give the signals for energy and PID analysis. The time constant τ_0 for each module can be changed by replacing 16 capacitor plugs (with five capacitors on each one). This permits reducing the pileup by using shorter τ_0 values for high counting rate applications at low energy

at some expense of the PID resolution.

(vii) Computer selectable gain adjustment for each channel. This is done via an IBM PC computer control of attenuation resistors between the two stages of the shaper.

(viii) A two-way DC coupled slow splitter providing the energy and the PID signals. The unattenuated branch is used to place the tail gate for PID by PSD. The E signal is obtained from the attenuated branch the magnitude of which is determined by a plug-in resistor pack. The attenuation factor was selected so that the channel numbers for the E and Tail signal be comparable for the range of particle to be detected. This in turn provides the optimal PID resolution. The DC coupling was found to be essential for achieving the desired counting rate stability.

(ix) A computer selectable monitor signal for the discriminator and energy signals of any specified channel. This is important for setting the gains and discriminator thresholds via a IBM PC computer. *This feature allows one to set up an experiment in 30–60 min!*

(x) A pileup sensing circuit is incorporated that provides a bit per channel if another pulse appears for a period $-\Delta t \rightarrow +\Delta t$ around the event trigger time. The interval is selectable and must end past the end of the tail gate. The pileup bit can then be used off line to identify events which include a pileup in any detector.

(xi) A time-to-FERA converter for each channel. This section provides a pulse of adjustable amplitude with a width determined by a common start pulse and the individual delayed discriminator signals. The delay time is set to a maximum of 800 ns to accommodate any adjustable desirable range for time measurement. The common start is derived from an overlap coincidence between the OR of all the CsI detectors and of all Ge or other external detectors and then is brought to each module via a LEMO input.

The module has one 16 pin input from the preamplifiers, one LEMO common start input, four LEMO outputs for the OR, multiplicity, discriminator monitor, and energy monitor signals. In addition there are four 16-channel multi-pin output connectors for the energy, the tail for PID, the time, and the pileup bits.

3.1.3. External logic

The external logic is used to prepare the coincidence gates. We need to OR together the discriminator OR's, create an overlap coincidence with the Ge OR's in a way that the Ge determines the timing. This AND is then fanned out to each bank for the TFC start. In addition, a second overlap coincidence is made with the Ge OR's such that the CsI determines the time. This AND is then used to make the E and tail gates for all the FERA ADCs.

3.2. Digitization and readout

The Microball signal digitization is done with 18 FERA ADC modules (LeCroy 4300B mod 610). There are 6 banks
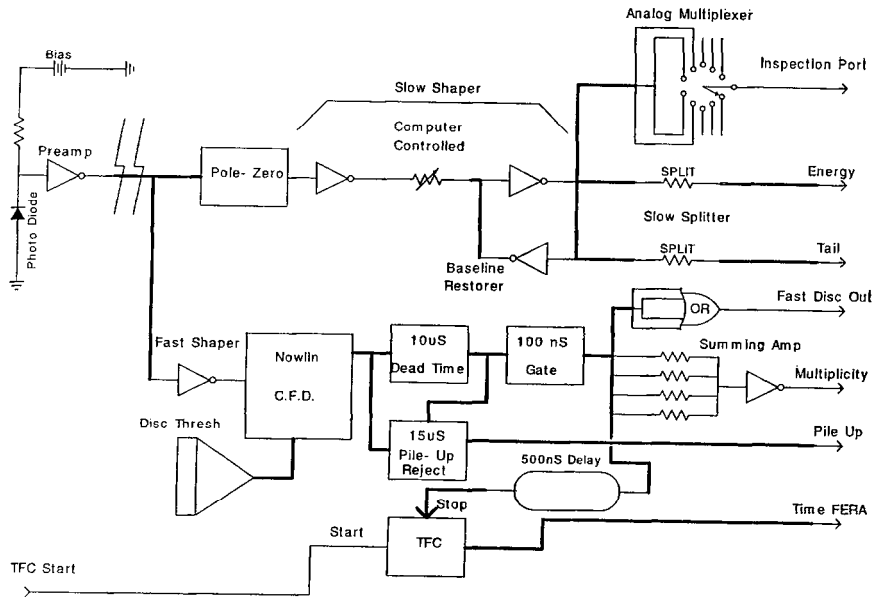
Fig. 14. Block diagram of the functions of the module for signal processing of the Microball CsI(Tl) detectors. The thin output lines refer to single Lemo connectors. The thick lines refer to 16-channel outputs on 32 pin connectors.

of 16 channels each. Each bank needs an energy, tail (PID), and a time signal ADC. The time-to-FERA converter has been designed in our module. The FERAs for the E, Tail analysis (PID), and the time have different gate widths. Therefore, three FERA bus driver modules have been used to set the gates and to control the handshaking for the ECL bus readout. In a recent modification the gates for each bank of 16 detectors was set separately by delay and gate generators and NIM to ECL converters. This reduces the noise level near the pedestals of the FERA ADCs that have to be processed.

The readout of the Microball information in full Gammasphere implementation is done by an Interface Module which reads the FERA ADCs via the ECl bus and attaches the information to the Gammasphere readout data stream.

Acknowledgements

References

[1] P.J. Nolan and P.J. Twin, Ann. Rev. Nucl. Part. Sci. 38 (1988) 533.
[2] R.V.F. Janssens and T.L. Khoo, Ann. Rev. Nucl. Part. Sci. 41 (1991) 321.
[3] D.W. Stracener, D.G. Sarantites, L.G. Sobotka, J. Elson, J.T. Hood, Z. Majka, V. Abenante, A. Chbihi, and D.C. Hensley, Nucl. Instr. and Meth. A 294 (1990) 485.
[4] D.W. Stracener, Ph.D. Thesis, Washington University, May 1993, (unpublished).
[5] C. Baktash et al., Phys. Lett. B 255 (1991) 174.
[6] P.-F. Hua, D.G. Sarantites, L.G. Sobotka, J.L. Barreto, and A. Kirov, Nucl. Instr. and Meth. A 330 (1993) 121.
[7] D.G. Sarantites et al., Phys. Rev. Lett. 64 (1990) 2129.
[8] R. Brun, F. Bruyant, M. Maire, A.C. McPherson and P. Zanarini, GEANT3 User's Guide, DD/EE/84-1, CERN (1987).
[9] R.T. DeSouza et al., Nucl. Instr. and Meth. A 295 (1990) 109.
[10] J.B. Birks, Theory and Practice of Scintillation Counting (Pergamon, New York, 1964) p. 457.
[11] B. Cederwall et al., Nucl. Instr. and Meth. A 354 (1995) 591.
[12] M. Devlin, D.G. Sarantites and L.G. Sobotka, Nucl. Instr. and Meth., in press.
[13] M. Ciric, J. Friese, H.J. Korner, and M.R. Maier (IEEE), and private communication.
[14] J. Elson, P.F. Hua, J.T. Hood, D.G. Sarantites, L.G. Sobotka and M.R. Maier, Nucl. Instr. and Meth., in press.
[15] C.H. Nowlin, Rev. Sci. Instr. 63 (1992) 2322.